

**Nonlinear photoassociation through exotic orbits**M. D. Forlevesi<sup>\*</sup> and R. Egydio de Carvalho<sup>†</sup>*Universidade Estadual Paulista–UNESP, Instituto de Geociências e Ciências Exatas–IGCE, Departamento de Estatística, Matemática Aplicada e Ciências da Computação, Rio Claro-SP 13506-900, Brazil*Emanuel F. de Lima<sup>‡</sup>*Departamento de Física, Universidade Federal de São Carlos, São Carlos-SP 13565-905, Brazil*

(Received 6 April 2021; accepted 13 June 2021; published 12 July 2021)

We investigate the effects of a particular kind of orbits, which we call exotic orbits, on the process of classical molecular photoassociation. As a starting model system, we consider the process described by the Morse potential with a time-dependent perturbation consisting of the interaction of an external laser field with the molecular dipole. When the external perturbation is turned off, the bound molecular states are classically represented by librational motion, whereas the unbound, the collisional states, are represented by unbound motion, and in both cases, the energy is a constant of motion. When the perturbation is turned on, the total energy is no longer a constant of motion and initial conditions in the unbound region can reach the bound region, and vice versa, through chaotic orbits. Alternatively, we have found that the connection between the bound and unbound sectors can be achieved through exotic orbits, which are comprised by librationlike parts, a localized chaotic region, and an unbounded constant-energy part. Thus, if a colliding atomic pair is in an exotic orbit, it penetrates a chaotic region coming from the unbound sector, subsequently performing librationlike motion, during which the molecule with constant bound energy is formed. Afterwards, the molecule returns to the chaotic region and from this region, it can either access a distinct bound energy or dissociate. We call this phenomenon, in which a metastable molecule is formed, intermittent photoassociation. We show that the key for the emergence of exotic orbits is the relatively short range of the dipole as compared to the interacting potential range. In order to further verify our results, we have considered realistic forms for the potentials and dipole functions of several molecules and found the emergence of exotic orbits, and consequently of intermittent photoassociation, for the MgLi and SrLi molecular parameters.

DOI: [10.1103/PhysRevE.104.014206](https://doi.org/10.1103/PhysRevE.104.014206)**I. INTRODUCTION**

Laser-induced photoassociation processes, in which two colliding atoms absorb or emit photons to create a molecule, is a topic of current scientific interest [1–4]. Together with photodissociation and molecular excitation, photoassociation is a fundamental phenomenon for the control of chemical reactions with a laser. Moreover, photoassociation is one of the possible routes for the formation of ultracold molecules [5] and Bose-Einstein molecular condensate [6].

The driven Morse oscillator is an important model that has been used in both quantum and classical scenarios for the study of photodissociation and photoassociation of diatomic molecules [7–12]. The classical approaches are motivated by at least two reasons: (i) to interpret the molecular dynamics from a classical, nonlinear point of view, since quantum-classical correspondence is found in many situations, and (ii) to understand the role of nonlinear mechanical forces exerted on particles interacting with a potential well [13]. The

unperturbed Morse oscillator has two distinct types of motion: libration, which corresponds to a bound vibrating molecule, and a free or colliding atomic pair, which corresponds to unbound motion. The threshold energy that separates the two kinds of motion defines the separatrix. The coupling between the molecular dipole and a time-dependent external field, produced by a laser, can produce transitions between these two energy regions. For a null external field, the phase space is filled by invariant tori and periodic orbits. As the amplitude of the external field increases, resonance islands, chaotic orbits, and periodic orbits coexist, and transitions between bound to unbound states can occur through chaotic routes [8].

Recently, we have proposed controlling photodissociation based on bent invariant tori, which cross the separatrix without being broken [9]. It has been shown that it is possible to deform an invariant torus to reach these two energy regions using high frequency and high amplitude of the external field. This fact opened up the possibility for inducing photodissociation through nonchaotic routes by means of appropriately designed pulses [14]. This deformed-tori mechanism can also be adapted to control photoassociation, but this route will not be pursued here.

In the present work, we investigate the laser pulse photoassociation using a nonlinear dynamics approach. We

<sup>\*</sup>forlevesi@gmail.com<sup>†</sup>Corresponding author: ricardo.egydio@unesp.br<sup>‡</sup>emanuel@df.ufscar.br

consider linearly polarized pulses, with the photoassociation occurring in the molecular electronic ground state and the laser-molecule interaction given in the dipole approximation. We assess this setting by considering ensembles of trajectories colliding with the Morse potential in the presence of external time-dependent pulses. The dipole coupling, which represents the molecule-field interaction, is given by a parametrized position-dependent function times the time-dependent harmonic pulse representing the laser electric field. The parameters of the dipole function allow for the control of the shape and the range of the interaction [15–17]. We observe that the unbound-bound transition can be performed through chaotic routes in a similar fashion to the known chaotic dissociation mechanism. Interestingly, we have found that for short-range interactions there are orbits consisting of a regular unbound part and a regular bound part coupled by a chaotic sea. We name such orbits, which present librationlike motion along with irregular motion, exotic orbits. Traveling in this kind of orbit, a colliding atomic pair approaches the region of interaction, coming from a locally unbound regular movement, and enters the chaotic region; then it can reach a locally bound trajectory with constant energy. Eventually, the molecule approaches the chaotic region again, from which it can access a distinct regular bound trajectory or dissociate. We call this process “intermittent photoassociation,” whose molecule is in a metastable state. Metastable states have been the subject of studies of different areas of science, for example, the formation of molecules produced by alkaline atoms, which may lead to the development of atomic clocks [18], and in the investigation of the properties of molecules such as ozone, hydrogen, helium, and others [19–21]. It was also observed that some properties of Bose-Einstein condensates [22–25] in diluted gases are due to the existence of molecular metastability [26]. Having these points in mind, we propose the use of pulses with appropriate duration to control the photoassociation process. The exotic orbits emerge in this context and support the partial photoassociation mechanism. These orbits are different from the chaotic ones that, while entering regions with stickiness, spend a long time performing near regular motions, and when they manage to escape they remain chaotic. Additionally, stickiness, in general, occurs around resonance islands where there are other small islands that trap the motion. The main difference here is that the exotic orbits occur independently of resonances and stickiness [27]. The trapping of trajectories when the rainbow angle exceeds a threshold in chaotic atom-surface scattering reported in [28] has some similarity with the mechanism described for the exotic orbits.

The paper is organized as follows. In Sec. II we present the theoretical approach for the Hamiltonian system; in Sec. III we present and discuss the theoretical results obtained, and in Sec. IV we apply our strategy to some real molecules in order to validate our approach. In Sec. V is the conclusion.

## II. MORSE PHOTOASSOCIATION MODEL

We consider the relative motion of a pair of colliding atoms in the presence of a linearly polarized laser field. For simplicity, we assume a head-on one-dimensional collision in the direction of the polarization of the laser. A suitable

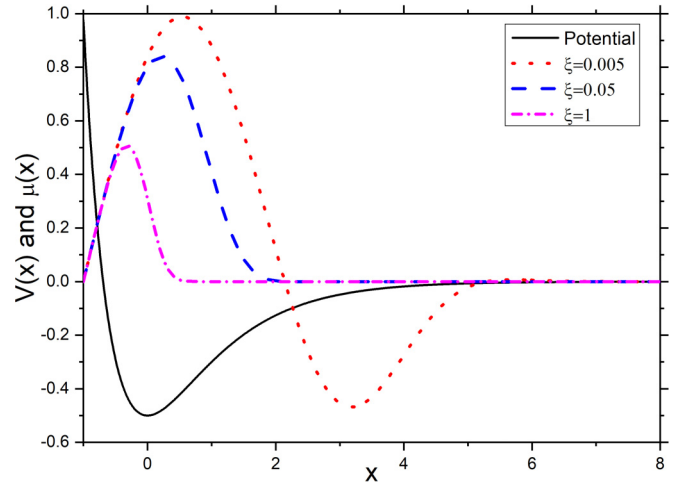


FIG. 1. Potential and dipole functions for  $\eta = 1.0$ ,  $x_e = 1.0$ . The solid black line corresponds to the Morse potential, the dotted red line corresponds to the long-range dipole  $\xi = 0.005$ , the dashed blue line to the medium-range dipole  $\xi = 0.05$ , and the short dash-dotted pink line to the short-range dipole  $\xi = 1.0$ .

unperturbed dimensionless Hamiltonian for describing the relative motion of the nuclei of a diatomic molecule is given by [29,30]

$$H_0(x, p) = \frac{p^2}{2} + V(x), \quad (1)$$

with  $V(x) = \frac{1}{2}(e^{-2x} - 2e^{-x})$  in which  $x$  is the distance between the nuclei and  $p$  is the conjugate linear momentum of the nuclei relative motion. The energy of the equilibrium point is  $-0.5$  and the separatrix is located at the energy  $V(x) = 0$ . For negative energy, the trajectories are bound, representing a vibrating molecule, and for positive energies, the trajectories are unbound, representing a free or colliding atomic pair.

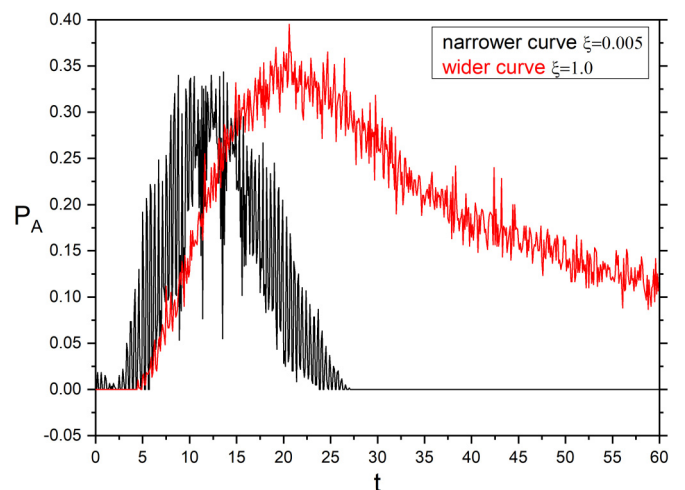


FIG. 2. Probability of photoassociation as a function of the laser pulse duration. The external field parameters are  $\varepsilon_0 = 11.0$ ,  $\Omega = 15.0$  and the dipole parameters are  $\eta = 1.0$ ,  $x_e = 1.0$ . The narrower curve corresponds to  $\xi = 0.005$  and the wider curve to  $\xi = 1.0$ . For both plots  $N_{\text{Traj}} = 600$ .

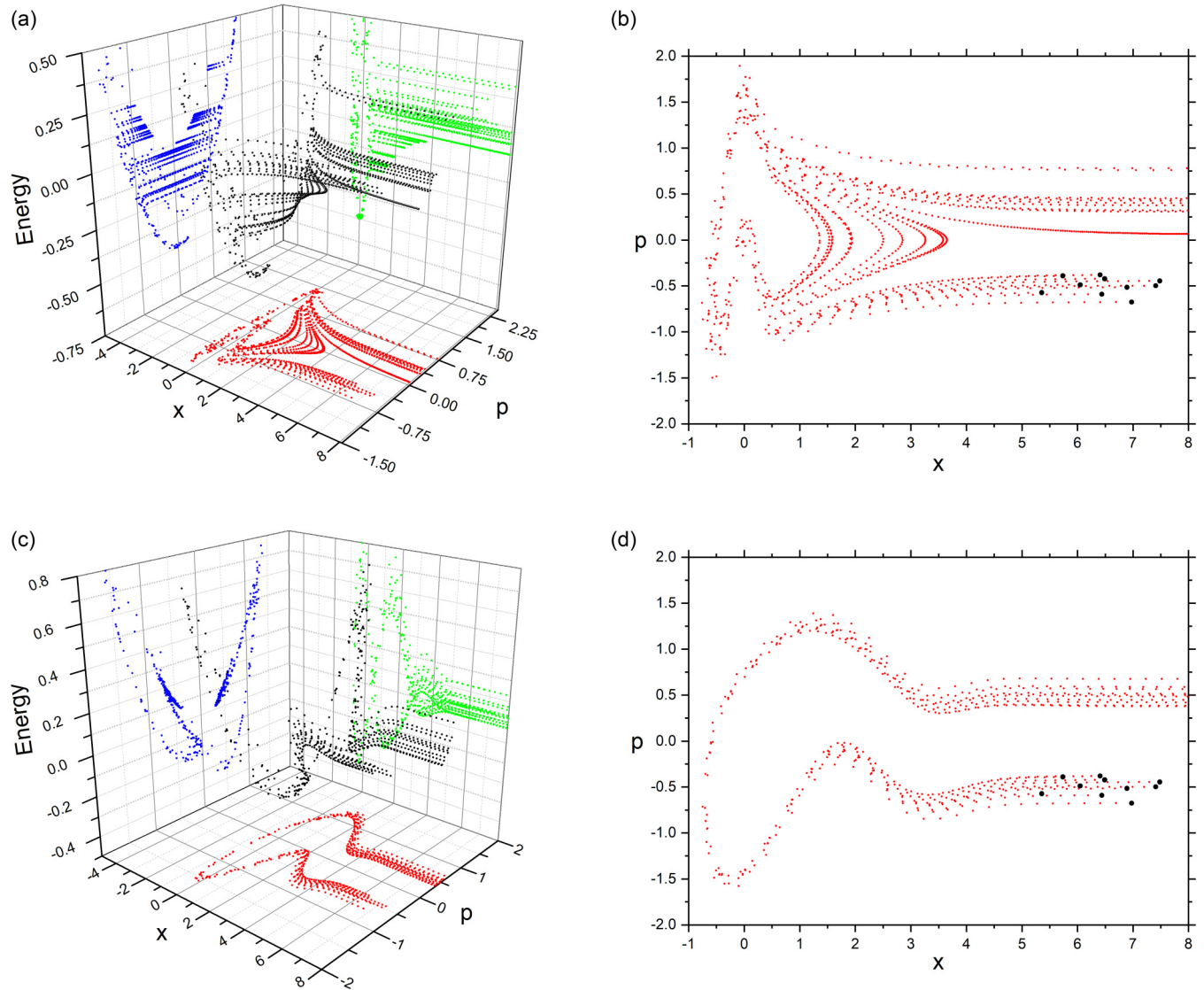


FIG. 3. Energy cube of the system for  $\Omega = 15.0$ ,  $\varepsilon_0 = 11.0$ ,  $\eta = 1.0$ , and  $x_e = 1.0$ . In (a)  $\xi = 1.0$  and in (c)  $\xi = 0.005$ . In (b), (d) we show the corresponding phase space  $(x, p)$ , the biggest dots (black) are the initial conditions. Dimensionless units are used.

The laser-molecule interaction is described in the dipole approximation by the term  $H_{\text{laser}}(x, t) = -\mu(x)\varepsilon(t)$ , where  $\varepsilon(t)$  is the time-dependent electric field of the laser and  $\mu(x)$  is the dipole moment of the molecule that is going to be formed. Here, we employ a functional form for the dipole, which allows us to control its shape and range through adjustable parameters,

$$\mu(x) = \frac{e^{-\xi(x+x_e)^4} \sin[\eta(x+x_e)]}{\eta}, \quad (2)$$

where  $\eta$ ,  $x_e$ , and  $\xi$  are the dimensionless adjustable parameters.

The dipole function given in Eq. (2) allows us to reproduce realistic dipole functions [31–34]. The parameter  $\eta$  controls the oscillatory behavior, the parameter  $\xi$  sets the range, and  $x_e$  gives the overall displacement of the dipole. In addition, it has been shown that the oscillatory behavior of the dipole

function can prevent trajectories from escaping the potential well, influencing the dynamics of the system [12].

The harmonic external electric field is written as

$$\varepsilon(t) = S(t) \varepsilon_0 \sin(\Omega t), \quad (3)$$

where  $\varepsilon_0$ ,  $\Omega$  are the amplitude and frequency of the laser and  $S(t)$  is given by

$$S(t) = \begin{cases} 1, & \text{if } 0 < t \leq t_f, \\ 0, & \text{otherwise} \end{cases}, \quad (4)$$

where  $t_f$  corresponds to the pulse duration.

The total Hamiltonian of the system is written as

$$H(x, p, t) = \frac{p^2}{2} + \frac{1}{2}(e^{-2x} - 2e^{-x}) - S(t) \frac{e^{-\xi(x+x_e)^4} \sin[\eta(x+x_e)]}{\eta} \varepsilon_0 \sin(\Omega t). \quad (5)$$

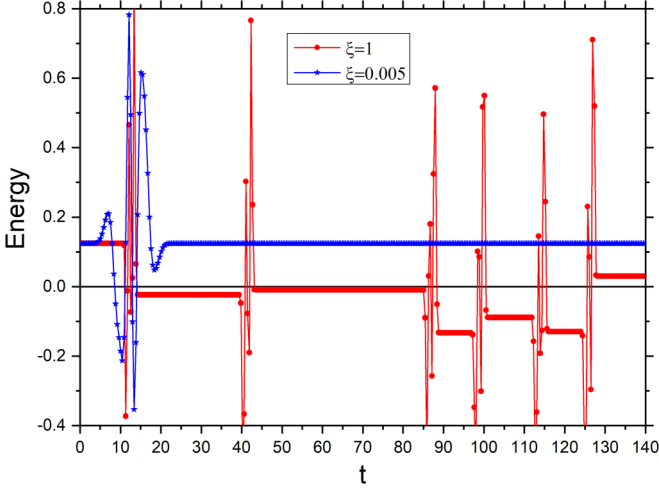


FIG. 4. The total energy of an initial condition as a function of time for  $\varepsilon_0 = 11.0$ ,  $\Omega = 15.0$ ,  $\eta = 1.0$ , and  $x_e = 1.0$ . The red dotted curve corresponds to  $\xi = 1.0$  and the blue curve with the star points corresponds to  $\xi = 0.005$ . The black line in  $E = 0$  is to guide the eyes. Dimensionless units are used.

Therefore, the ensemble of trajectories colliding with the Morse potential under the action of an external field, governed by the Hamiltonian (5), accounts for the classical photoassociation dynamics induced by laser pulses.

### III. RESULTS FROM THE MORSE MODEL

The probability of photoassociation is strongly dependent on the choice of the parameters of the external field; therefore, after evaluating different combinations, we defined our approach with  $\varepsilon_0 = 11$  and  $\Omega = 15$ , which led to an expressive photoassociation. We consider three different dipole functions, one with the long range defined by  $\xi = 0.005$ , the other with the intermediary range  $\xi = 0.05$ , and the last with the short range given by  $\xi = 1$ . For all scenarios we used  $\eta = 1.0$  and  $x_e = 1.0$ . Figure 1 shows the comparison between the potential range (black solid line) and the three dipole functions: (i) the long-range dipole (dotted red line) which has a range up to  $x \sim 5.0$ , (ii) the medium-range dipole (dashed blue line) which has a range up to  $x \sim 2.0$  and, (iii) the short-range dipole (short dash-dotted pink line) which has a range up to  $x \sim 0.3$ .

As presented in previous work [12], we define the photoassociation probability  $P_A$  as the ratio of the number of trajectories  $n$  that remain trapped in the Morse potential after the action of a laser pulse, by the total number of trajectories

TABLE I. Range of potential and dipole function. Dimensionless units are used.

	$\Delta\alpha_V = \alpha_V - R_e$	$\Delta\alpha_\mu = \alpha_\mu - R_e$	$\delta = \frac{\Delta\alpha_\mu}{\Delta\alpha_V}$
$\xi = 1.0$	6.38	0.56	0.09
$\xi = 0.05$	6.38	2.35	0.37
$\xi = 0.005$	6.38	7.75	1.21

$N_{\text{Traj}}$ ,

$$P_A = \frac{n}{N_{\text{Traj}}}, \quad (6)$$

and we call these trapped trajectories photoassociated trajectories.

The ensembles of initial conditions are chosen to follow a Gaussian distribution, in analogy with a colliding wave packet in the quantum version of the model [29,35,36]. In practice, we employ a Monte Carlo technique using a normalized distribution given by [37]

$$\rho(x, p) = \left( \frac{1}{4\pi\delta} \right) e^{-\frac{\beta}{2}(x-x_0)^2 - \frac{(p-p_0)^2}{8\beta\delta^2}}, \quad (7)$$

where  $x_0$  and  $p_0$  are the wave packet average position and momentum, respectively;  $\delta$  and  $\beta$  are adjustable parameters which define the width of the Gaussian in the phase space. Note that for large  $\beta$  and small  $\delta$  the distribution is concentrated around  $x_0$  and  $p_0$ ; we set  $\beta = 0.12$  and  $\delta = 0.2$  in all calculations. The procedure to distribute the phase-space points is as follows: Take  $y = \sqrt{\beta/2}(x - x_0)$  and  $z = (p - p_0)\sqrt{8\beta\delta^2}$ , where  $y = r\cos(\theta)$  and  $z = r\sin(\theta)$ , with  $\theta = 2\pi\Gamma$  and  $r = \sqrt{-\ln(1-\zeta)}$ . The points of the phase space are found by providing values for the pair  $(\zeta, \Gamma)$  uniformly distributed between  $[0, 1]$ . The initial conditions  $x_0$  and  $p_0$  corresponding to each pair  $(\zeta, \Gamma)$  are distributed according to Eq. (7). Figure 2 shows the photoassociation probability as a function of the laser pulse duration  $t_f$  for the short- and the long-range dipoles, and setting  $N_{\text{Traj}} = 600$ ,  $x_0 = 7.0$ ,  $p_0 = -0.5$  as the photoassociation probability  $P_A$  is essentially the same up to  $t_f \approx 15.0$ . However, from this time, the  $P_A$  for the long-range (narrower curve) dipole decreases very fast, while the  $P_A$  for the short-range (wider curve) dipole increases up to  $t_f = 20$  and then decreases relatively slowly, reaching 0.15 at  $t_f \approx 60$ . The time duration of the laser pulse has an important role in the behavior of the photoassociation probability because the final energy of the trajectory, after the perturbation action, is extremely sensitive to the choice of the final time. We also observe that for the long-range dipole

TABLE II. Parameters of the equilibrium point, potential range, dipole range, and the ratio between the ranges.  $R_e$ ,  $\alpha_V$ ,  $\alpha_\mu$  are in atomic units.

	$R_e$	$\alpha_V$	$\alpha_\mu$	$\Delta\alpha_V = \alpha_V - R_e$	$\Delta\alpha_\mu = \alpha_\mu - R_e$	$\delta = \frac{\Delta\alpha_\mu}{\Delta\alpha_V}$
MgLi	5.72586	20.00	13.66	14.27414	7.92914	0.55549
SrLi	6.708852726	24.96	18.20	18.25147274	11.49147274	0.63
CaLi	6.42506831	25.01	30.00	18.58493164	23.574931464	1.2685
HF	2.35055	6.71	7.367	4.97740142	6.370	1.279
HCL	2.4085748	7.31	9.233	4.901403	6.814403	1.40

TABLE III. Parameters of Eqs. (8)–(10) for the potentials.  $R_e$  and  $D_e$  are in atomic units.

	$R_e$	$D_e$	$\beta_0$	$\beta_1$	$\beta_2$	$\beta_3$
SrLi	6.70852726	0.0101871	4.0069261	2.1016080	-1.23119	0.3212922
MgLi	5.725869745	0.007097047	4.069261	0.64016080	-0.0519	0.0112922

the photoassociation exists only for a range of  $t_f \approx [1.0 : 26]$  and has the maximum value of  $P_A \approx 0.32$  for  $t_f \approx 12.5$ . On the other hand, for the short-range dipole the photoassociation occurs for  $t_f > 5.0$ , with a maximum of  $P_A \approx 0.40$  for  $t_f \approx 20.0$ . Note that for the short-range dipole, the probability of photoassociation is higher compared to the long-range dipole and it provides greater freedom in managing the pulse duration time.

It is important to emphasize that after carrying out several tests it was possible to verify the existence of intermittent photoassociation for the medium-range dipole as well, which shows that the occurrence of the exotic orbits is associated with the range of the dipole. Therefore, we will mention the medium-range dipole scenario only when it is convenient. If we employ a pulsed laser field instead of a continuous wave field (cw), the details of the dynamics will certainly suffer some influence. However, we expect that the exotic orbits will continue to exist but eventually will be more difficult to observe since additional frequencies will appear around the carrier frequency of the pulse. It is worth commenting that studies on ultracold atoms trapped in periodically shaken optical lattices [38] show some correspondence with our approach, due to the possibilities we have to change the shape of the laser and the effects of finite width time pulses that we consider.

In order to understand what causes this change in the characteristic of the photoassociation probability, it is interesting to analyze the time evolution of the trajectories in the phase space. To ensure that the trajectory is well represented in the phase space, we need to use a long-time laser pulse. We observed that the time  $t_f = 140$  is enough for this purpose in Figs. 3(b) and 3(d). To prevent the phase space from having a dense number of points, which would be difficult to visualize, we use a smaller number of trajectories,  $N_{\text{Traj}} = 10$  and we keep the average position and momentum  $x_o = 7.0$ ,  $p_o = -0.5$ . We solve the Hamilton equations with the fourth-order Runge-Kutta method of fixed step  $h = 10^{-4}$ . For each period that the term  $\sin(\Omega t)$  is zero, in Hamiltonian equation (5), we store the points  $(x, p, E_0)$  where  $E_0$  is the unperturbed energy of the system. With these data we plot a three-dimensional graphic known as an *energy cube*.

The energy cube was introduced in [9]. In that work we selected some level curves of the system governed by the Hamiltonian (1) and we plotted the energies of some librational tori and of a few open curves corresponding to

free orbits. The projections on the planes  $(H_0, x)$  and  $(H_0, p)$  evidence that the total energy of the system is a global constant of motion for the unperturbed system. We call this three-dimensional (3D) plot as *energy cube*. Subsequently we used this idea for the perturbed system in which the total energy is no longer constant in motion. In the energy cube, in the presence of the perturbation, the only plotted points are the ones in which  $t = n \frac{2\pi}{\Omega}$ , that is, for multiple times of the laser field period, which results in  $H(t = n \frac{2\pi}{\Omega}) = H_0$ . Then, we consider the Poincaré stroboscopic map of the system. Concerning the current work, Figs. 3(a) and 3(c) are the energy cubes for the total Hamiltonian given in Eq. (5). In these energy cubes, the black dots represent the 3D movement of the initial conditions, the true trajectories; the blue dots are the projections of the movement on the plane (Energy,  $p$ ); the green dots represent the projections on the plane (Energy,  $x$ ); and finally, the red dots are the projections on the plane  $(x, p)$ , that is, in the phase space. From these plots, we can easily identify when the energy is constant and when it is not by observing the projections corresponding to the blue and green points. The red projection, or Figs. 3(b) and 3(d), show the corresponding phase spaces with and without exotic orbits. Thus, Fig. 3 is particularly important in understanding the dynamics and in choosing the parameters.

The respective energy cubes for the long-range dipole,  $\eta = 1.0$ ,  $x_e = 1.0$ ,  $\xi = 0.005$ , and with short range,  $\eta = 1.0$ ,  $x_e = 1.0$ ,  $\xi = 1.0$  are presented in Fig. 3, as well as the trajectories in the associated phase space. The red projection of Fig. 3(a) shows that, for the short-range dipole, the motion is trapped in stable regions of constant energy despite the variation in position and momentum for some interval of time. That constant-energy regime is characteristic of the exotic orbit. These states can also be observed in the blue plane  $(p, \text{Energy})$  between the energies  $[-0.2 : 0]$ . In Fig. 3(b) we see that the exotic orbits (metastable states) are in phase space between  $x \approx [0.5 : 4.0]$  and  $p \approx [-1.0 : 1.0]$ . On the other hand, this phenomenon is not observed for the long-range dipole in Figs. 3(c) and 3(d). It is worth noting that a similar dynamic to this one, which we call exotic orbits, was reported in [39] but in a different context. In order to detect the exotic orbits, several tests have been carried out by changing the laser parameters and the initial conditions, which showed that they generally occur for initial conditions that have initial energy values close to the separatrix energy and for intense and high-frequency fields. For instance, from the 600 initial

TABLE IV. Parameters of Eq. (11) for the molecular dipoles. Atomic units were used.

	$\alpha_1$	$\alpha_2$	$\alpha_3$	$\alpha_4$	$\alpha_5$	$\alpha_6$	$a$	$b$	$R_0$	$C$
SrLi	59.8065	-56.382	21.3226	-4.1561	0.44262	-0.0245	-0.3300	-0.3832	9.71	0.42
MgLi	-46.947	36.3473	-10.852	1.59382	-0.1163	0.00339	2.2803	0.84370	7.2	5.88

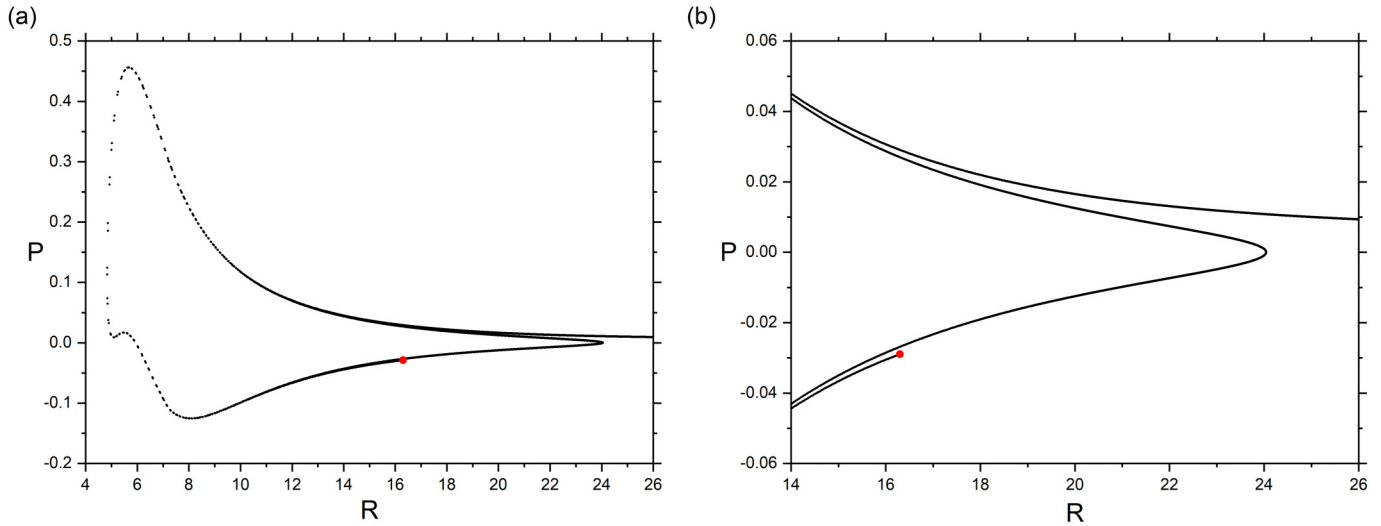


FIG. 5. In (a) we show the phase space  $(R,P)$  for the molecule MgLi with  $\Omega = 5.0$ ,  $\varepsilon_0 = 4.38$ , and  $R_e = 5.725\ 86$ . In (b) we show an amplification of the phase space. The red circles are the initial conditions. Atomic units were used.

conditions used to build Fig. 2, we selected only ten and built the respective energy cubes [Figs. 3(a) and 3(c)] and the phase space [Figs. 3(b) and 3(d)].

To see the details of the observed temporary trapping, we consider in Fig. 4 a single trajectory starting from  $(x_0, p_0) = (7.0, -0.5)$  and analyze its energy over the time interval  $t = [0, 140]$ . The blue curve with star points (long-range dipole) shows that the trajectory starts with positive energy, collides with the potential around  $t \sim 11$ , spends a short time with oscillating energy between positive and negative values, and then escapes the influence of the potential, around  $t \sim 15$ , with the same positive initial energy. On the other hand, the red dotted curve (short-range dipole) shows that the particle remains trapped in the well, around  $t \sim 15$  up to  $t \sim 40$ , identified by the first plateau; from  $t \sim 40$  it oscillates again with positive and negative energies until  $t \sim 45$ ; thereafter it is trapped in a second large negative energy plateau until

$t \sim 85$ , and experiences a third oscillation up to  $t \sim 88$ ; in the range  $t: [\sim 88: \sim 97]$  the third negative plateau occurs. Next the particle oscillates once again in the interval  $t: [\sim 97\text{--}\sim 100]$ ; in the range  $t: [\sim 101: \sim 110]$  the fourth negative plateau occurs. Next the particle oscillates once again in the interval  $t: [\sim 110\text{--}\sim 117]$ ; in the range  $t: [\sim 117: \sim 125]$  the fifth negative plateau occurs; next the particle oscillates once again in the interval  $t: [\sim 125\text{--}\sim 128]$  and from there it dissociates.

Therefore, for the short-range nonlinear dipole, there are five plateaus of constant energy, or metastable states, which are regions where the system could be approximated by a nonperturbed Hamiltonian with constant negative energy corresponding to trapped trajectories. This phenomenon corroborates the behavior of the photoassociation probability as a function of the time duration of the laser pulse seen in Fig. 2. For the long-range dipole, there is a short window of time to induce photoassociation, whereas for the short-range dipole,

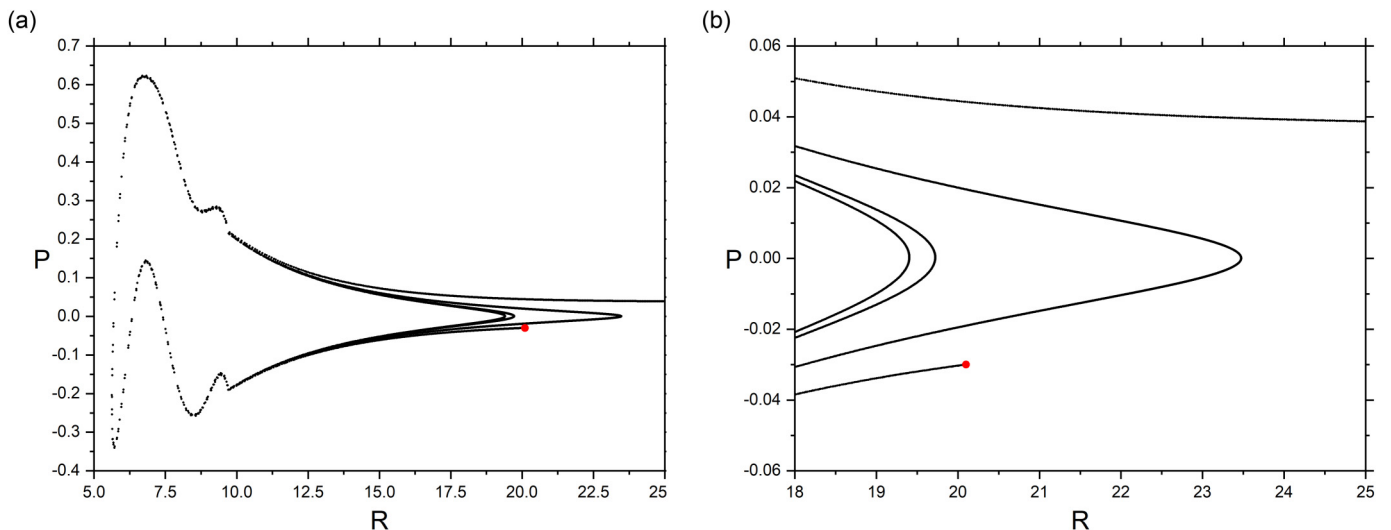


FIG. 6. In (a) we show the phase space  $(R,P)$  for the molecule SrLi with  $\Omega = 5.0$ ,  $\varepsilon_0 = 22.0$ , and  $R_e = 6.708\ 852\ 726$ . In (b) we show an amplification of the phase space. The red circles are the initial conditions. Atomic units were used.

the time window is relatively long, encompassing periods of constant energy. Based on this behavior, in the short-range dipole case, the use of laser pulses with duration set in the first constant-energy plateau will maximize the photoassociation probability. Thus, the ratio  $\delta$ , between the molecular dipole range and the potential range, will be a reference parameter for our analysis.

We define the range of the potential as being  $\Delta\alpha_V = \alpha_V - R_e$  and the molecular dipole  $\Delta\alpha_\mu = \alpha_\mu - R_e$ , where  $R_e$  represents the equilibrium point of the potential (in this generic case,  $R_e = 0$ ). We define  $\alpha_\mu$  when the dipole reaches 0.1% of its maximum extension; this is  $\alpha_\mu = 0.001 \times \mu_{\text{MAX}}$ . Similarly,  $\alpha_V = 0.001 \times V_{\text{MAX}}$ . In this way, we build a table for the three dipole ranges.

The results of Table I show that the phenomenon of partial photoassociation is more evident when the ratio between the range of the dipole and the range of the potential is less than 1; that is,  $\delta < 1$ . We will take this theoretical result into consideration and verify if this criterion occurs for more realistic molecular models.

To illustrate the relevant time for the interaction process, we present a simple calculation for the period of the highest negative energy of an exotic orbit showed in Fig. 3(b). First, we numerically calculate its energy, which is  $E = -0.02561$ . Next, we use this energy to calculate the associated action for the unperturbed system, through  $J = 1 - \sqrt{-2H_0} = 0.7737$ , so that the unperturbed oscillation frequency is  $\omega = (1 - J) = 0.2263$ , and then the corresponding oscillation period is  $T = 28.56$ . The period of the perturbation is merely  $T = 2\pi/\Omega = 2\pi/15 = 0.41$ . For Fig. 2 the duration of the perturbation is  $t = 60$  and for Fig. 4,  $t = 140$ ; that is, we allow the system to evolve some periods of the perturbation but corresponding to a short interaction time in comparison with  $T = 28.56$ .

#### IV. RESULTS FOR REALISTIC MOLECULAR PARAMETERS

In this section, we explore the existence of exotic orbits and intermittent photoassociation for the molecules hydrogen chloride—HCl, hydrogen fluoride—HF, lithium magnesium—MgLi, calcium lithium—CaLi, and strontium lithium—SrLi. We have constructed the molecular potentials and dipole functions based on *ab initio* data obtained from the literature. Atomic units are used throughout this section.

In order to describe the molecular potentials of diatomic molecules we have followed Ref. [40], in which the author proposed an extended Lennard-Jones potential, which proved to be a high-precision low-parameter model. The potential function assumes the form

$$V(R) = D_e \left[ 1 - \left( \frac{R_e}{R} \right)^{n(R)} \right]^2, \quad (8)$$

which can be described in a polynomial expansion [41], with  $R$  and  $R_e$  being the relative internuclear positions and the equilibrium point in dimensional coordinates. According to [40] the best choice for  $n(R)$  and the values of the parameters and constants is

$$n(R) = \beta_0 + \beta_1 \zeta + \beta_2 \zeta^2 + \beta_3 \zeta^3, \quad (9)$$

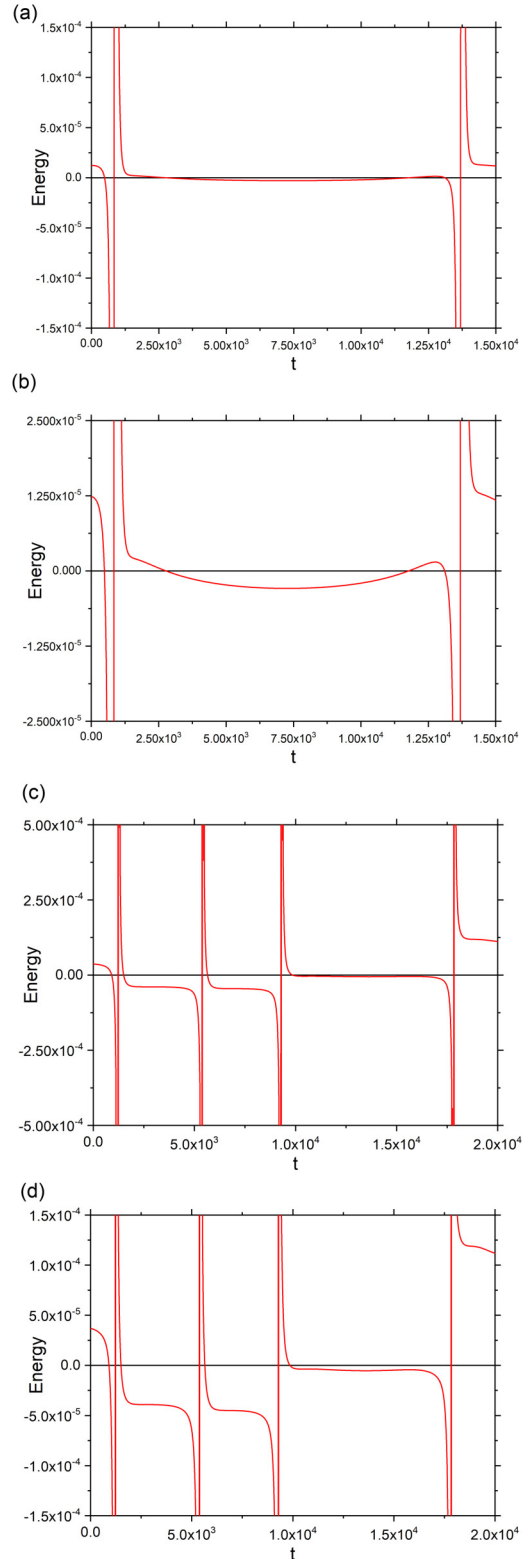


FIG. 7. The total energy of an initial condition as a function of time. In (a) we show the energy for the molecule MgLi from the initial condition  $x_0 = 16.30$  and  $p_0 = -0.027$ . In (b) we show the same of (a) in an amplified scale. In (c) we show the energy for the molecule SrLi from the initial condition  $x_0 = 20.10$  and  $p_0 = -0.07$ . In (d) we show the same of (c) in an amplified scale. The black straight lines in  $E = 0$  are to guide the eyes. Atomic units were used.

in which

$$\zeta = \frac{R - R_e}{z^q R + R_e}, \quad z = \frac{R - R_e}{R + R_e}, \quad \text{and} \quad q = \begin{cases} 4, & \text{if } R > R_e \\ 6, & \text{if } R < R_e \end{cases} \quad (10)$$

In order to describe the molecular permanent dipole of the real molecules, a semiempirical method in the form of a piecewise-continuous function has been used, which exhibits correct behaviors for small and large internuclear separations and agrees with the dipole moment value close to the equilibrium position between the nuclei of the atoms. For the HCl and HF molecules, we use the dipole moment function and the value of the parameters proposed in [34].

The dipole moment functions for the molecules SrLi, MgLi, and CaLi are obtained in Ref. [31] using a finite field perturbation theory. We fitted these dipoles using the piecewise function described by

$$\mu(R) = \begin{cases} \sum_{n=1}^6 \alpha_n R^n, & \text{if } R < R_0 \\ C e^{a+bR}, & \text{if } R > R_0 \end{cases}, \quad (11)$$

in which  $\alpha_n$ ,  $a$ ,  $b$ , and  $C$  are numerically adjustable parameters, while  $R_0$  is the numerical crossover point between the polynomial and the exponential forms. Table II shows all the parameters involved. In Table II, we show the calculated ranges and the parameter  $\delta$  for several molecules. We note that the MgLi and SrLi molecules present  $\delta$  smaller than 1, whereas the CaLi, HCl, and HF molecules have  $\delta$  greater than 1. Then, based on the results of the previous section, for the Morse potential, the existence of metastable states would be possible only for the molecules MgLi and SrLi. To evaluate this condition, we study the dynamics in the phase space for these two molecules with the corresponding potentials as well as the time evolution of the energy. The constants involved in the fitted potentials and dipole moments are shown in Tables III and IV.

After checking different parameters for the external field and for the initial conditions, we found the exotic orbits that led to intermittent photoassociation for the two molecules MgLi and SrLi. In Figs. 5 and 6 we show the phase space for both molecules, respectively, and the time range of the external field described by Eq. (3) with  $t_f = 4 \times 10^4$ . Only one initial condition is shown, which has positive initial energy.

In Fig. 5 we see one branch of regular motion for the MgLi molecule and in Fig. 6 we note three branches of regular

motion for the SrLi molecule, which leads us to expect to see one and three plateaus in the time evolution of the system energy. In order to verify this situation, we consider only one initial condition for each molecule and calculate the energy time evolution. The results are presented in Fig. 7.

Figures 7(a) and 7(b) show that for the MgLi molecule the initial condition is trapped in only one plateau that is located between  $t$  [ $\sim 2500$ :  $\sim 12\,500$ ]. Figures 7(c) and 7(d) show that for the SrLi molecule the initial condition is trapped in three plateaus of negative energy, the first between  $t$  [ $\sim 2000$ :  $\sim 4000$ ], the second between  $t$  [ $\sim 6000$ :  $\sim 8000$ ], and the third between  $t$  [ $\sim 10\,000$ :  $\sim 17\,000$ ].

## V. CONCLUSION

In this work, we have investigated the classical photoassociation of diatomic molecules. We have initially considered the driven Morse oscillator accounting for the process. For different sets of parameters, we have observed molecular photoassociation. In particular, for short-range dipole functions, we have found that the photoassociation mechanism is not the usual chaotic one, but it occurred with some constant bound energies separated by chaotic bursts. The mechanism for such intermittent photoassociation was supported by what we have called exotic orbits. Regular librationlike parts and a regular unbound-motion part, which are connected by a chaotic section, comprise these orbits. We observe that this intermittent photoassociation is a mechanism that leads to metastable molecules. We point out that if the laser field is turned off while the molecule has negative energy, it becomes a stable and permanent molecule. We have verified that these exotic orbits, and consequently the intermittent photoassociation, exist in more realistic molecular models, provided the range of the dipole interaction is sufficiently short as compared to the corresponding potential.

## ACKNOWLEDGMENTS

We acknowledge support from the Brazilian scientific agency CAPES—Coordination for the Improvement of Higher Education Personnel. R.E.d.C. and E.F.d.L. also thank CNPQ—National Council for Scientific and Technological Development through Grants No. 306034/2015-8 and No. 423982/2018-4, and FAPESP—São Paulo Research Foundation through Grants No. 2019/07329-4 and No. 2014/23648-9, respectively.

- [1] K. M. Jones, E. Tiesinga, P. D. Lett, and P. S. Julienne, Ultracold photoassociation spectroscopy: Long-range molecules and atomic scattering, *Rev. Mod. Phys.* **78**, 483 (2006).
- [2] C. P. Koch and M. Shapiro, Coherent control of ultracold photoassociation, *Chem. Rev.* **112**, 4928 (2012).
- [3] E. F. de Lima, T. S. Ho, and H. Rabitz, Optimal laser control of molecular photoassociation along with vibrational stabilization, *Chem. Phys. Lett.* **501**, 267 (2011).
- [4] J. Ulmanis, J. Deiglmayr, M. Repp, R. Wester, and M. Weidemüller, Ultracold molecules formed by photoassociation:

Heteronuclear dimers, inelastic collisions, and interactions with ultrashort laser pulses, *Chem. Rev.* **112**, 4890 (2012).

- [5] W. C. Stwalley, and He Wang, Photoassociation of ultracold atoms: A new spectroscopic technique, *J. Mol. Spectroscopy* **195**, 194 (1999).
- [6] T. Gasenzer, Photoassociation dynamics in a Bose-Einstein condensate, *Phys. Rev. A* **70**, 043618 (2004).
- [7] A. K. de Almeida, Jr., R. Egidio de Carvalho, and E. F. de Lima, Controlling dissociation by trapping trajectories in highly energetic states, *Physica A* **449**, 101 (2016).

- [8] E. F. de Lima, T. N. Ramos, and R. E. de Carvalho, Role of the range of the dipole function in the classical dynamics of molecular dissociation, *Phys. Rev. E* **87**, 014901 (2013).
- [9] M. D. Forlevesi, R. Egidio de Carvalho, and E. F. de Lima, A tunable mechanism to control photo-dissociation with invariant tori with variable energies, *Physica A (Amsterdam, Neth.)* **490**, 681 (2018).
- [10] R. C. Brown and R. E. Wyatt, Barriers to chaotic classical motion and quantum mechanical localization in multiphoton dissociation, *J. Phys. Chem.* **90**, 3590 (1986).
- [11] A. Sethi and S. Keshavamurthy, Local phase space control and interplay of classical and quantum effects in dissociation of a driven Morse oscillator, *Phys. Rev. A* **79**, 033416 (2009).
- [12] S. D. Schwartz, Vibrational energy transfer from resummed evolution operators, *J. Chem. Phys.* **101**, 10436 (1994).
- [13] C. Chandre, J. Mahecha, and J. P. Salas, Driving the formation of the RbCs dimer by a laser pulse: A nonlinear-dynamics approach, *Phys. Rev. A* **95**, 033424 (2017).
- [14] E. F. de Lima, R. E. de Carvalho, and M. D. Forlevesi, Non-chaotic laser pulse dissociation through deformed tori, *Phys. Rev. E* **101**, 022207 (2020).
- [15] W. T. Zemke, W. C. Stwalley, S. R. Langhoff, G. L. Valderrama, and M. J. Berry, Radiative transition probabilities for all vibrational levels in the  $X^1\Sigma^+$  state of HF, *J. Chem. Phys.* **95**, 7846 (1991).
- [16] A. Guldberg and G. D. Billing, Laser-induced dissociation of an anharmonic oscillator coupled to a set of harmonic oscillators, *Chem. Phys. Lett.* **186**, 229 (1991).
- [17] E. F. de Lima and R. Egidio de Carvalho, Effects of oscillatory behavior of the dipole function on the dissociation dynamics of the classical driven Morse oscillator, *Physica D (Amsterdam, Neth.)* **241**, 1753 (2012).
- [18] G. Cappellini, L. F. Livi, L. Franchi, D. Tusi, D. Benedicto Orenes, M. Inguscio, J. Catani, and L. Fallani, Coherent Manipulation of Orbital Feshbach Molecules of Two-Electron Atoms, *Phys. Rev. X* **9**, 011028 (2019).
- [19] W. Lichten, Metastable hydrogen molecules, *Phys. Rev.* **120**, 848 (1960).
- [20] D. Babikov, B. K. Kendrick, R. B. Walker, and R. T. Pack, Metastable states of ozone calculated on an accurate potential energy surface, *J. Chem. Phys.* **118**, 6298 (2003).
- [21] A. V. Phelps, Absorption studies of helium metastable atoms and molecules, *Phys. Rev.* **99**, 1307 (1955).
- [22] M. H. Anderson, J. R. Ensher, M. R. Matthews, C. E. Wieman, and E. A. Cornell, Observation of Bose-Einstein condensation in a dilute atomic vapor, *Science* **269**, 198 (1995).
- [23] K. B. Davis, M.-O. Mewes, M. R. Andrews, N. J. van Druten, D. S. Durfee, D. M. Kurn, and W. Ketterle, Bose-Einstein Condensation in a Gas of Sodium Atoms, *Phys. Rev. Lett.* **75**, 3969 (1995).
- [24] C. C. Bradley, C. A. Sackett, and R. G. Hulet, Bose-Einstein Condensation of Lithium: Observation of Limited Condensate Number, *Phys. Rev. Lett.* **78**, 985 (1997).
- [25] T. C. Killian, D. G. Fried, L. Willmann, D. Landhuis, S. C. Moss, T. J. Greytak, and D. Kleppner, Cold Collision Frequency Shift of the  $1S - 2S$  Transition in Hydrogen, *Phys. Rev. Lett.* **81**, 3807 (1998).
- [26] H.-J. Miesner, D. M. Stamper-Kurn, J. Stenger, S. Inouye, A. P. Chikkatur, and W. Ketterle, Observation of Metastable States in Spinor Bose-Einstein Condensates, *Phys. Rev. Lett.* **82**, 2228 (1999).
- [27] G. Contopoulos and M. Harsoula, Stickiness in chaos, *Int. J. Bifurcation Chaos* **18**, 2929 (2008).
- [28] S. Miret-Artés, R. Guantes, J. Margalef-Roig, F. Borondo, and C. Jaffé, Classical singularities in chaotic atom-surface scattering, *Phys. Rev. B* **54**, 10397 (1996).
- [29] Y. Gu and J.-M. Yuan, Classical dynamics and resonance structures in laser-induced dissociation of a Morse oscillator, *Phys. Rev. A* **36**, 3788 (1987).
- [30] J. Heagy and J. M. Yuan, Dynamics of an impulsively driven Morse oscillator, *Phys. Rev. A* **41**, 571 (1990).
- [31] G. Gopakumar, M. Abe, M. Kajita, and M. Hada, *Ab initio* study of permanent electric dipole moment and radiative lifetimes of alkaline-earth-metal-Li molecules, *Phys. Rev. A* **84**, 062514 (2011).
- [32] R. Guérout, M. Aymar, and O. Dulieu, Ground state of the polar alkali-metal-atom-strontium molecules: Potential energy curve and permanent dipole moment, *Phys. Rev. A* **82**, 042508 (2010).
- [33] M. A. Buldakov, V. N. Cherepanov, E. V. Koryukina, and Y. N. Kalugina, On some aspects of changing the sign of the dipole moment functions of diatomic molecules, *J. Phys. B: At., Mol. Opt. Phys.* **42**, 105102 (2009).
- [34] M. A. Buldakov and V. N. Cherepanov, The semiempirical dipole moment functions of the molecules HX ( $X = \text{F, Cl, Br, I, O}$ ), CO and NO, *J. Phys. B: At., Mol. Opt. Phys.* **37**, 3973 (2004).
- [35] J.-M. Yuan and W.-K. Liu, Classical and quantum dynamics of chirped pulse dissociation of diatomic molecules, *Phys. Rev. A* **57**, 1992 (1998).
- [36] M. E. Goggin and P. W. Milonni, Driven Morse oscillator: Classical chaos, quantum theory, and photodissociation, *Phys. Rev. A* **37**, 796 (1988).
- [37] E. F. de Lima, Control of chaotic photoassociation in the driven Morse oscillator, in *5th International Conference on Physics and Control-PHYSCON 2011*, Leon, Spain, 2011.
- [38] F. Revuelta, R. Chacón, and F. Borondo, Dynamical localization in nonideal kicked rotors, *Phys. Rev. E* **98**, 062202 (2018).
- [39] R. Egidio de Carvalho and A. M. Ozório de Almeida, Integrable approximation to the overlap of resonances, *Phys. Lett. A* **162**, 457 (1992).
- [40] P. G. Hajigeorgiou, An extended Lennard-Jones potential energy function for diatomic molecules: Application to ground electronic states, *J. Mol. Spectrosc.* **263**, 101 (2010).
- [41] J. L. Dunham, The energy levels of a rotating vibrator, *Phys. Rev.* **41**, 721 (1932).